

Evaluation of Autofocus Algorithms for Automatic Detection of *Caenorhabditis elegans* Lipid Droplets*

ZHANG Xiang^{1,2)**}, JIA Ce²⁾, XIE Kang²⁾

¹⁾ College of Life Science and Technology, Huazhong University of Science and Technology, Wuhan 430074, China;

²⁾ Institute of Biophysics, Chinese Academy of Sciences, Beijing 100101, China)

Abstract Autofocusing is a fundamental step towards automated microscopic screening of *Caenorhabditis elegans*. Determining the optimal focus in an optical microscope is based on a clarity-evaluation function that is applied to images acquired from different focuses of the same field. The maximum value of the function is considered as the point of optimal focus. In this paper, 16 autofocus algorithms which were collected from well-known algorithms as well as the most recently proposed focusing algorithms have been evaluated. Through these evaluations, an optimal algorithm was found for *C. elegans* lipid droplets to set up an automatic screening system. Many features were assessed in this paper, for instance accuracy, computational time, addition of noise, and focusing curve. Our results have shown that most of the algorithms show an overall high performance for this type of image, and absolute Tenengrad algorithm will be our first choice for its best performance considering accuracy.

Key words *C. elegans* lipid droplets, autofocus algorithms, automatic screening

DOI: 10.16476/j.pibb.2015.0189

Caenorhabditis elegans (*C. elegans*) is an established model organism for studying lipid droplets and energy metabolism because it has many advantages. For example, its mutation is simple to use as genetic tool, and it is easily to be examined in microscope^[1]. In the past few years, owing to the identification of lipid droplet-associated proteins such as DHS-3^[1] and PLN^[2], lipid droplets can be marked with fluorescence protein-tagged as a fat storage indicator. RNA interference (RNAi) has been investigated in *C. elegans* since 1998 by Fire *et al.* (Nobel Prize in Physiology or Medicine in 2006)^[3]. Through an RNAi screen, uncharacterized fat storage regulatory genes can be identified in *C. elegans*^[2, 4-6]. However, manual identification and counting of *C. elegans* lipid droplets is exhausting and time-consuming. Moreover, it requires a trained operator, and presents a high false-negative rate. Therefore, in order to reduce this rate and speed up the process, automatic screening is necessary.

Focusing is a fundamental and crucial step in automatic system. Determining the optimal focus in an

optical microscope is based on a clarity-evaluation function that is applied to images acquired from different focuses of the same field^[7]. The maximum value of the function is regarded as the point of optimal focus. Many autofocus algorithms have been proposed in the literature, but their accuracy can vary depending on contents of the processed images. According to the previous studies, Santos *et al.*^[8] compared autofocus algorithm in molecular cytogenetic, and drew the conclusion that the method Vollath-4 is the most appropriate for FISH (fluorescence *in situ* hybridization) images. Osibote *et al.*^[9] determined that method Vollath-4^[10] has the best focus accuracy for tuberculosis in bright-field microscopy. However, other studies such as Kimura *et al.*^[11] found that method variance provided the best overall performance

*This work was supported by a grant from The National Natural Science Foundation of China (31300701).

**Corresponding author.

Tel: 86-10-64888522, E-mail: zhangxiang@moon.ibp.ac.cn

Received: June 23, 2015 Accepted: December 22, 2015

for tuberculosis. Liu *et al.*^[12] drew the same conclusion in both blood smear and pap smear. Redondo *et al.*^[13] claimed that variance, normalized variance and Vollath-5 are the most suitable method for automatic system in bright-field microscopy pathology. Furthermore, the study by Mateos-Pérez *et al.*^[14] included additional assessing features such as variability of the fluorescent microscopy images, addition of noise, illumination changes, and prefiltering processes.

This paper focuses on the ascertainment of the optimal autofocus algorithms for *C. elegans* lipid droplets fluorescence imaging through a systematic evaluation of 16 commonly-used autofocus algorithms. A set of criteria, such as accuracy error, computation time, the number of local maxima, FWHM (full width at half maximum) of the focus curve and the noise robustness, were assessed to evaluate the performance of the autofocus algorithms. In the previous literature, optimally focused image was identified by trained operators, which will lead to a little uncertainty and inaccuracy, because different observers could choose slightly different images around the optimal focus plane. For example, Osibote *et al.*^[9] determined that method Vollath-4 has the best focus accuracy for tuberculosis, whereas Kimura *et al.*^[11] found that method variance provides the best overall performance for tuberculosis. Therefore, we adopted an objective way to determine the optimal focus plane in this paper to avoid subjective deviation.

1 Materials

Strains P_{vha-6::dhs-3::GFP} (single copy) were created by professor Ho Yi Mak (Hong Kong University of Science and Technology). DHS-3 can be used as a lipid droplet marker protein in *C. elegans*, as well as a fat storage indicator in live worms. This marker protein will facilitate further mechanistic studies of lipid droplets in *C. elegans*^[1]. All strains were maintained on NGM plates under standard conditions^[15].

Worms were raised at approximately 22°C and prepared for imaging as described previously^[16]. Briefly, the worms were soaked in a solution of 0.1% tricaine and 0.01% levamlsole (Sigma-Aldrich) in M9 for 20~30 min prior to imaging^[17]. The immobilized worms were then transferred with a glass hook to a slab of 3% agarose in M9. The coverslip was then sealed with Vaseline.

Images were acquired using a motorized Zeiss Imager M2 Microscope equipped with AxioCam CCD camera (Carl Zeiss, Germany) and X-Cite 120Q light source (Lumen Dynamics, Canada) driven by Axiovision (Carl Zeiss, Germany). Green fluorescence images were acquired with the resolution of 1388 × 1040 pixels and 16bits of dynamic range in grayscale. A trained operator selected the best focal plane from which 30 images were captured upward in axial direction and another 29 downward, thus the stacks are made of 60 images. Two different magnifications were used: ×10 (*NA* = 0.30) and ×40 (*NA* = 0.75). Different magnification used different *Z* step: $\Delta Z = 0.5 \mu\text{m}$ at ×40, and $\Delta Z = 2 \mu\text{m}$ at ×10. Ten stacks were captured with two different magnifications each from ten different worms. All algorithms implemented in Matlab 7.6.0 (The Mathworks, America) on an Intel Core i5 3.50 GHz 16 GB RAM computer using the Windows 8 operating system (Microsoft, America).

2 Autofocus methods

Autofocus is characteristic of automatic system. There are two kinds of autofocus methods: active methods and passive methods. Active methods are based on measuring the distance between the lens and object of the scene by emitting ultrasonic or infrared waves^[13]. But these methods have limitations in case of live model organisms such as *C. elegans*. Passive methods are grounded on analyzing the image sharpness of the objects by autofocus functions, which are usually related to high frequencies of the image.

The autofocus function gives a mathematical value that shows the degree of focus for each image of the same sample. The fundamental assumption behind most of the functions is that a defocused image results from convolution of the image with a certain point spread function (PSF), which usually produces a decrease in the high frequencies of the image^[8]. This result can also be regarded as the assumption that focused images contain more information and detail than defocus images. The sixteen autofocus functions analyzed in this study can be classified into five groups: (1) Derivative-Based function, (2) Transform-Based function, (3) Statistics-Based function, (4) Histogram-Based function and (5) Intensity-Based function. For an image of size $M \times N$, the notation $g(x, y)$ refers to the image intensity at point (x, y) , while the symbol \otimes indicates the convolution operator.

2.1 Derivative-based function

These functions are based on a derivative suppose that defocused images usually have less high-frequency content than focused images.

Brenner gradient (BREN). This function calculates the first difference between a pixel and its neighbor two points away^[18].

$$AF_{\text{BREN}} = \sum_x \sum_y |g(x, y+2) - g(x, y)|^2 \quad (1)$$

While $|g(x, y+1) - g(x, y)| \geq \tau$ (threshold value)

Laplacian (LAP). This focus function was originally used to find focusing errors caused by noise^[19]. The algorithm implements the image convolution with a discrete Laplacian mask as follows:

$$AF_{\text{LAP}} = \sum_x \sum_y [g(x-1, y) + g(x+1, y) + g(x, y-1) + g(x, y+1) - 4g(x, y)]^2 \quad (2)$$

Tenengrad (TEN). This algorithm convolves an image with Sobel operators and then it sums the square of all the magnitudes greater than a threshold value^[20-22].

$$AF_{\text{TEN}} = \sum_x \sum_y [g(x, y) \otimes S]^2 + [g(x, y) \otimes S']^2, \quad \forall g(x, y) > \tau \quad (3)$$

Where S and S' are the Sobel's kernel and its transpose respectively, where S is given by:

$$S = \begin{bmatrix} 1 & 0 & -1 \\ 2 & 0 & -2 \\ 1 & 0 & -1 \end{bmatrix} \quad (4)$$

Absolute Tenengrad (ATEN). This focus function is similar to the previous Eq(3), but the absolute value of the gradient coefficients is used in order to reduce the computation time^[23].

$$AF_{\text{ATEN}} = \sum_x \sum_y |g(x, y) \otimes S| + |g(x, y) \otimes S'| \quad (5)$$

Gaussian filter (GS). This focus function is based on a gradient filter derived from convolving the image with a first-order Gaussian derivative^[24].

$$AF_{\text{GS}}(\sigma) = \frac{1}{MN} \sum_x \sum_y [g(x, y) \otimes G_x(x, y, \sigma)]^2 + [g(x, y) \otimes G_y(x, y, \sigma)]^2 \quad (6)$$

Where G_x and G_y are the first-order Gaussian derivatives in the x and y directions. The σ parameter of the Gaussian method should be adjusted in relation to the objects present in the image. We evaluated different σ values to test the robustness of the method. Here we set $\sigma=1$.

2.2 Transform-based function

Transform-based functions are utilized to calculate the degree of focusing for each image by a

mathematical transform.

Discrete Cosine Transform (DCT). Focusing techniques based on band-passed filters perform well. In this algorithm, images are divided into blocks of 40×40 pixels then DCT is applied, and the sum of four band-pass diagonal bands representing mid and high frequencies is chosen^[25]:

$$C(u, v) = \frac{1}{16} \sum_x \sum_y g(x, y) \cos\left(\frac{\pi(2m+1)u}{2M}\right) \cos\left(\frac{\pi(2n+1)v}{2N}\right) \quad (7)$$

Midfrequency-DCT (MDCT). The influence of the band-pass DCT coefficients on the focus measure has been analyzed^[26]. A 4×4 convolution mask for extracting the central coefficient $C(4, 4)$ of the DCT, which is used as a focus measurement. The MDCT operator can be calculated as:

$$AF_{\text{MDCT}} = \sum_x \sum_y (g(x, y) \otimes O_{\text{MDCT}})^2 \quad (8)$$

With

$$O_{\text{MDCT}} = \begin{bmatrix} 1 & 1 & -1 & -1 \\ 1 & 1 & -1 & -1 \\ -1 & -1 & 1 & 1 \\ -1 & -1 & 1 & 1 \end{bmatrix} \quad (9)$$

Wavelet transformation (WT). This function is based on discrete wavelet transformation. The wavelet focus function calculates ratio of the energy in low and high pass bands^[27].

$$AF_{\text{WT}} = \frac{\|h_w(f)\|}{\|l_w(f)\|} \quad (10)$$

Where $h_w(f)$ is the discrete wavelet transformation in high pass band, and $l_w(f)$ is the discrete wavelet transformation in the low pass band.

2.3 Statistics-based function

Statistics-based functions use features such as variance and autocorrelation to calculate the degree of focusing for each image.

Variance (VAR). This function computes the variations in the gray level among the image pixels, where bright and dark pixels have the same influence^[28].

$$AF_{\text{VAR}} = \frac{1}{MN} \sum_x \sum_y [g(x, y) - \bar{g}]^2 \quad (11)$$

Where $\bar{g} = \frac{1}{MN} \sum_x \sum_y g(x, y)$ is the image mean.

Normalized variance (NVAR)^[28]. This function is a variation of Eq(11) by normalizing with the mean \bar{g} , which compensates for changes in the average image brightness.

$$AF_{\text{NVAR}} = \frac{1}{MN\bar{g}} \sum_x \sum_y [g(x, y) - \bar{g}]^2 \quad (12)$$

Vollath-4 (VOL4) [29-30]. This algorithm proposed by Vollath is based on an autocorrelation function.

$$AF_{VOL4} = \sum_x \sum_y^{M-1} g(x, y) \cdot g(x+1, y) - \sum_x \sum_y^{M-2} g(x, y) \cdot g(x+2, y) \quad (13)$$

Vollath-5 (VOL5) [29-30]. Vollath proposed a modification of Eq(13) which is based on the standard deviation function.

$$AF_{VOL5} = \sum_x \sum_y^{M-1} g(x, y) \cdot g(x+1, y) - MNg^2 \quad (14)$$

2.4 Histogram-based function

These functions are grounded on the assumption that focused images have a greater number of grey levels than defocused images[31].

Log-histogram (LOG). Image histogram approximates a probability distribution function of gray levels, where the variance of this distribution increases as the image sharpness increases too[13]. This algorithm is based on the bright pixels in the image by multiplying the variance by the logarithm function:

$$AF_{LOG} = \sum_l [l - E_{\log}\{l\}]^2 \cdot \log(p_l) \quad (15)$$

Where p_l is the probability if the intensity level l and $E_{\log}\{l\} = \sum_l l \cdot \log(p_l)$ is the expected value of the log-histogram.

Weighted histogram (WHS). Images focused under fluorescence illumination present higher portions of pixels with bright gray levels than unfocused image. This recently proposed algorithm is based on a weighted image histogram without introducing a constant threshold[32].

$$AF_{WHS} = \sum_l [\sqrt[5]{h(l)} \cdot l^5 \cdot 10^{-15}] \quad (16)$$

2.5 Intensity-based function

Intensity of the image is another feature that characterizes the degree of focusing. It can be estimated with different ways.

Power squared (PS). This focus function sums all image intensities[8].

$$AF_{PS} = \sum_x \sum_y g(x, y)^2 \quad (17)$$

Threshold (TH). This function sums the number of pixels above a threshold as follows[28]:

$$AF_{TH} = \sum_x \sum_y T_{\tau}[g(x, y)] \quad (18)$$

With

$$T_{\tau} = \begin{cases} 1 & \text{if } g(x, y) > \tau \\ 0 & \text{otherwise} \end{cases} \quad (19)$$

We used a fixed threshold at 50% of maximum brightness value in the whole stack.

3 Results

3.1 Accuracy error and computational time

Because the Z-axis step is small, it is hard to distinguish the best focused image around the focus plane for human observers. Different observers could choose slightly different images around the focus plane. So the assessment of autofocus algorithms would be slightly different from different observers. In this paper, we adopted an objective way to determine the optimal focus plane to avoid subjective deviation. Autofocus functions were computed for each stack. The focus plane calculated by each function was not the same. Therefore, we defined the focus point as the point which most algorithms are considered as the focus point. We compared the focus point obtained by most algorithms and human observers. The results are shown in Table 1. Because of the cases are similar in both $\times 10$ and $\times 40$, only the data at $\times 40$ is shown in the

Table 1 Comparison of most algorithms and human observers at $\times 40$

	Most algorithms (frame)	Human observer1 (frame)	Deviation1 (frame)	Human observer2(frame)	Deviation2 (frame)
Stack1	32	33	1	32	0
Stack2	32	32	0	32	0
Stack3	32	32	0	34	2
Stack4	34	33	-1	33	-1
Stack5	31	32	1	33	2
Stack6	37	38	1	36	-1
Stack7	30	31	1	30	0
Stack8	31	30	-1	30	-1
Stack9	33	33	0	34	1
Stack10	34	35	1	34	0

present work.

The deviation with the focus point was considered as the focus error for each algorithm. The errors of the algorithms applied to the ten stacks are shown in Figure 1. The variance of data was indicated by the

lines drawn above the bars. The stacks acquired at different focus points using a constant Z step ($\Delta Z = 0.5 \mu\text{m}$ at $\times 40$, $\Delta Z = 2 \mu\text{m}$ at $\times 10$). The error of the algorithm (sum of average and variance) less than one step indicates that the algorithm has high performance.

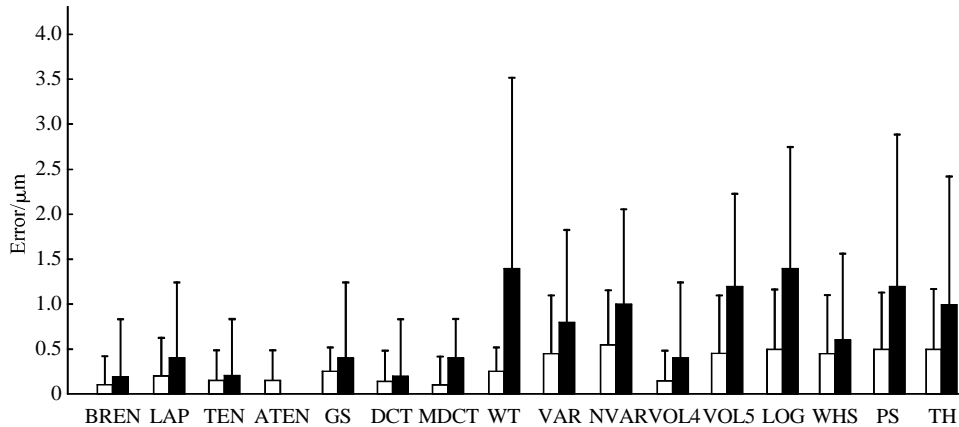


Fig. 1 Error according to magnification value
 □ : $\times 40$ (NA=0.75); ■ : $\times 10$ (NA=0.30).

According to the plots, ATEN, BREN, DCT, WT, MDCT, GS, TEN show high performance at $\times 40$ (less than $0.5 \mu\text{m}$ which indicates 1 frame distance), while ATEN, BREN, DCT, MDCT, LAP, GS, TEN, VAR, VOL4, WHS show high performance at $\times 10$ (less than $2 \mu\text{m}$ which indicates 1 frame distance). So ATEN,

BREN, DCT, MDCT, GS, TEN show high performance at both magnifications. Furthermore, ATEN achieves the best accuracy of all algorithms. In addition, the percentage of correctly focused images was computed and show in Figure 2.

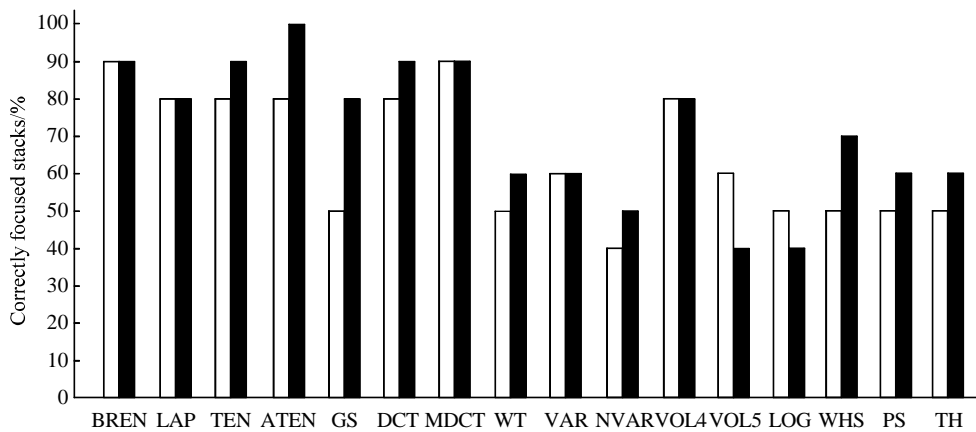


Fig. 2 Percentage of images correctly focused
 □ : $\times 40$ (NA=0.75); ■ : $\times 10$ (NA=0.30).

Computational time and accuracy in automatic systems is a trade-off and the algorithms with the best ranking in computational time are not necessarily effective in accuracy (Figure 3). Autofocus functions implemented in Matlab 7.6.0 (The Mathworks, America) on an Intel Core i5 3.50 GHz 16 GB RAM

computer using the Windows 8 operating system (Microsoft, America). According to the evaluated algorithms, the TH method was the fastest with 5.28 ms per image and the WT method was the slowest with 289.65 ms per image.

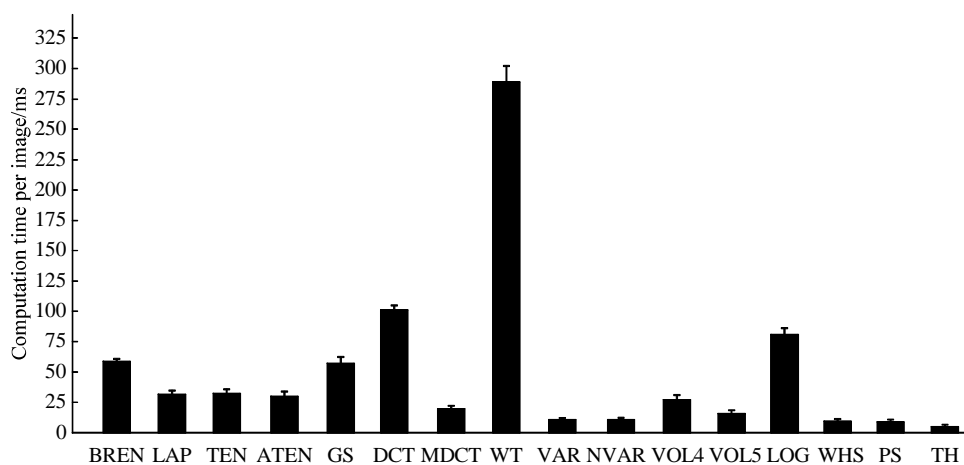


Fig. 3 Mean computation time required by each algorithm per image

3.2 Noise responses

The performance of autofocus function has been evaluated when different levels of noise are added to the stacks. We have added increasing levels of white Gaussian noise to the original data(Figure 4). Although the used values are not the real experiment conditions, this test can give additional information about the robustness of the algorithms. We calculated their influence in the accuracy error and the results for noise robustness are summarized in Figure 5. It is noticed that most of the algorithms are relatively stable until the distortion becomes very large, with the exception of WT which demonstrate more sensibility to noise than other algorithms.

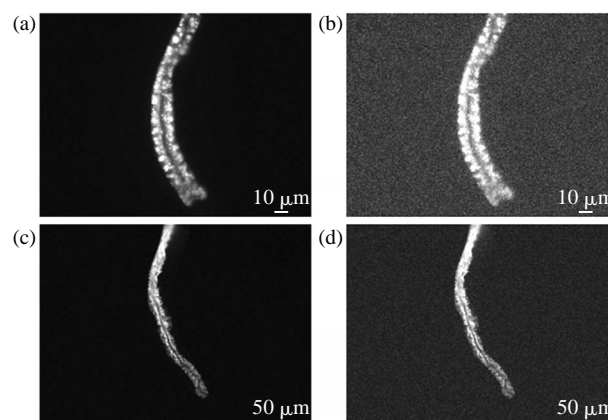


Fig. 4 *C. elegans* lipid droplets fluorescence images used in evaluation

(a) $\times 40$ focused image. (b) $\times 40$ focused image with 80 dBW Gaussian noise. (c) $\times 10$ focused image. (d) $\times 10$ focused image with 80 dBW Gaussian noise.

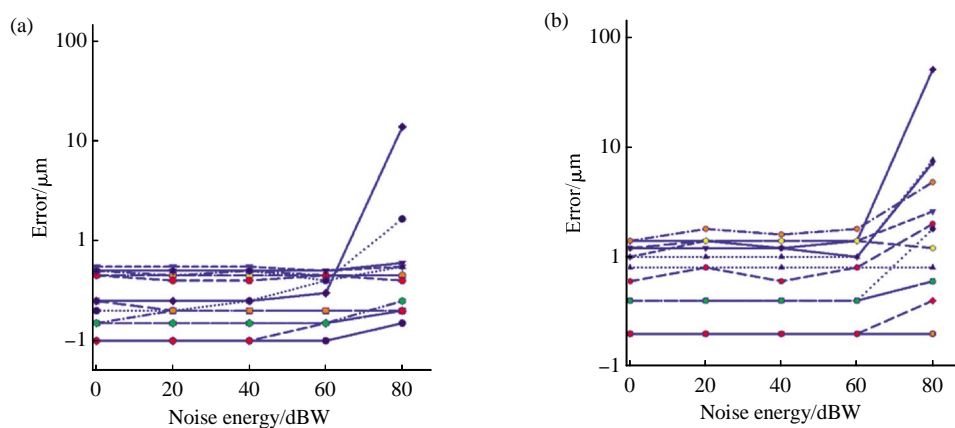


Fig. 5 Responses of algorithms to white Gaussian noise at $\times 40$ (a) and $\times 10$ (b)

Because the value of ATEN is 0, 0, 0, 0, 0.2 here, it doesn't show in the logarithmic coordinate. —●—: BREN; —●—: LAP; —▼—: TEN; —▲—: ATEN; —■—: GS; —■—: DCT; —◆—: MDCT; —◆—: WT; —▲—: VAR; —▼—: NVAR; —●—: VOL4; —●—: VOL5; —●—: LOG; —●—: WHS; —▼—: PS; —▲—: TH.

3.3 Accuracy in focus curve

The reliable and fast autofocusing method is an important aspect in the automatization system and the shape of the focus curve can play an influential role in this aspect. The focus function should be unimodal in theory, but in fact it can present diverse local maxima which can affect the convergence of the autofocus procedure. Moreover, the focus curve should be sharp at the peak, which can speed up the convergence of the procedure. In order to characterize the autofocus

algorithms more completely, we take into account two aspects: the number of local maxima and the width at 50% maximum of the focus curve (FWHM, full width at half maximum).

First, we can see in Figure 6 that most algorithms present a unique maximum except PS. In terms of the width ratio of the focus curve, (Figure 7), ATEN, BREN, DCT, WT, MDCT, LAP, GS, TEN, VOL4, WHS show high performance both at $\times 40$ (less than $10\ \mu\text{m}$) and at $\times 10$ (less than $40\ \mu\text{m}$).

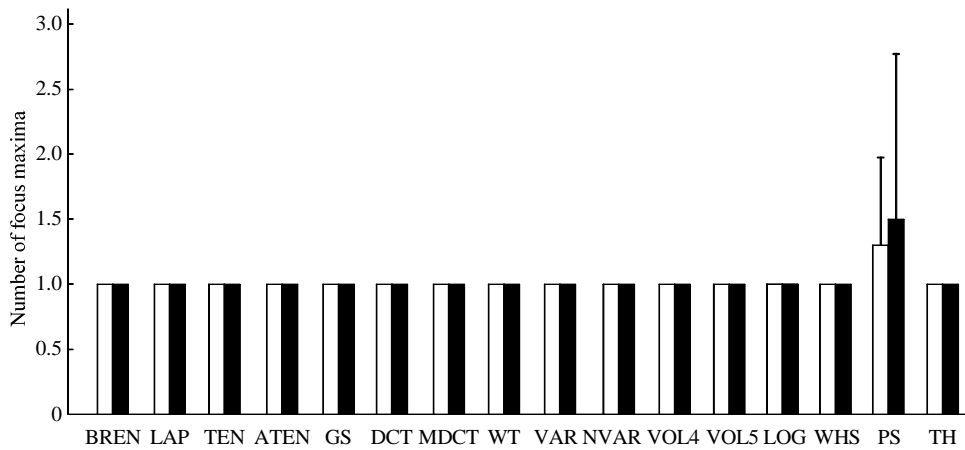


Fig. 6 Comparison of focus algorithms in terms of averaged number of local maxima (included the global maximum)
 □ : $\times 40$ (NA=0.75); ■ : $\times 10$ (NA=0.30).

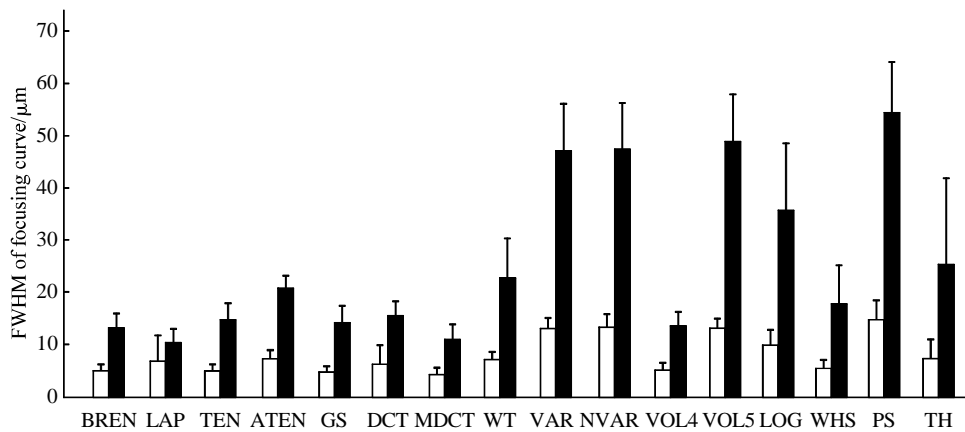


Fig. 7 Comparison of focus algorithms in terms of average FWHM of the focus curve
 □ : $\times 40$ (NA=0.75); ■ : $\times 10$ (NA=0.30).

4 Discussion

Identifying the gene which related to fat metabolism in *C. elegans* is a laborious and time-consuming task. Therefore, automatic screening system, from image acquisition to analysis, will be

beneficial to the gene identification in *C. elegans*. We have presented here a study of autofocus algorithms for automatic detection of *C. elegans* lipid droplets in fluorescence images.

From the results, most of the algorithms show a low accuracy error. Especially, ATEN, DCT, MDCT,

GS, TEN show high performance at both magnification $\times 40$ and $\times 10$. So they could be regarded as suitable algorithms for a *C. elegans* automatic system. Moreover, ATEN achieves the best accuracy of all algorithms for *C. elegans* lipid droplets. In the presence of noise, most of the algorithms do not change noticeably except WT. These results show that most of the algorithms are quite robust and independent of noise. In addition, most of the algorithms show no false maxima except PS. In terms of the width ratio of the focus curve, ATEN, BREN, DCT, WT, MDCT, LAP, GS, TEN, VOL4, WHS show high performance at both magnification $\times 40$ and $\times 10$.

To sum up, in our study WT show a poor accuracy, and has a long computational time, so it is not suitable for *C. elegans* lipid droplets, although WT may have a good performance in other applications. Comprehensive consideration of accuracy and computational time, we recommend ATEN, MDCT and TEN for *C. elegans* lipid droplets. Moreover, ATEN achieves the best accuracy. In an automatic screening system, we often require both high accuracy and fast acquisition. In this case, we can apply the fastest algorithm TH for rough search, and then apply ATEN algorithm for fine search.

Acknowledgments We thank professor Ho Yi Mak (Hong Kong University of Science and Technology) for P_{vh}a-6::dhs-3::GFP strains. We also thank professor XU Tao (Institute of Biophysics, Chinese Academy of Sciences) for the comments on the manuscript.

References

- [1] Zhang P, Na H, Liu Z, *et al.* Proteomic study and marker protein identification of *Caenorhabditis elegans* lipid droplets. *Mol Cell Proteomics*, 2012, **11**(8): 317–328
- [2] Liu ZL, Xun H. A lipid droplet-associated GFP reporter-based screen identifies new fat storage regulators in *C. elegans*. *J Genet Genomics*, 2014, **41**(5): 305–313
- [3] Fire A, Xu S Q, K.Montgomery M, *et al.* Potent and specific genetic interference by double-stranded RNA in *Caenorhabditis elegans*. *Nature*, 1998, **391**(6669): 806–811
- [4] Guo Y, Walther T C, Rao M, *et al.* Functional genomic screen reveals genes involved in lipid-droplet formation and utilization. *Nature*, 2008, **453**(7195): 657–661
- [5] Wang M C, Min W, Freudiger C W, *et al.* RNAi screening for fat regulatory genes with SRS microscopy. *Nat Methods*, 2011, **8**(2): 135–138
- [6] Zhang Y, Zou X, Ding Y, *et al.* Comparative genomics and functional study of lipid metabolic genes in *Caenorhabditis elegans*. *BMC Genomics*, 2013, **14**: 164
- [7] Klmuira A, Costa M G F, Filho C F F C, *et al.* Evaluation of autofocus functions of conventional sputum smear microscopy for tuberculosis//32nd Annual International Conference of the IEEE EMBS 2010, 2010
- [8] Santos A, Solórzano C O D, Vaquero J J, *et al.* Evaluation of autofocus functions in molecular cytogenetic analysis. *J Microscopy*, 1997, **188**(3): 264–272
- [9] Osibote O A, Dendere R, Krishnan S, *et al.* Automated focusing in bright-field microscopy for tuberculosis detection. *J Microsc*, 2010, **240**(2): 155–163
- [10] Vollath D. The influence of the scene parameters and of noise on the behavior of automatic focusing algorithms. *J Microsc*, 1988, **151**(2): 133–146
- [11] Kimura A, Costa M G F, Filho C F F C, *et al.* Evaluation of autofocus functions of conventional sputum smear microscopy for tuberculosis//2010 International Conference of the IEEE Engineering in Medicine and Biology Society, Engineering in Medicine and Biology Society, Buenos Aires, 2010: 3041–3044
- [12] Liu X Y, Wang W H, Sun Y. Dynamic evaluation of autofocus-ing for automated microscopic analysis of blood smear and papa smear. *J Microsc*, 2007, **227**(1): 15–23
- [13] Redondo R I, Bueno G, Valdiviezo J C, *et al.* Autofocus evaluation for brightfield microscopy pathology. *Biomed Opt*, 2012, **17**(3): 036008
- [14] Mateos-Pérez J M, Redondo R, Nava R, *et al.* Comparative evaluation of autofocus algorithms for a real-time system for automatic detection of Mycobacterium tuberculosis. *Cytometry*, 2012, **81**(3): 213–221
- [15] Brenner S. The genetics of *Caenorhabditis elegans*. *Genetics*, 1974, **77**(1): 71–94
- [16] McCarter J, Bartlett B, Dang T, *et al.* On the control of oocyte meiotic maturation and ovulation in *Caenorhabditis elegans*. *Dev Biol*, 1999, **205**(1): 111–128
- [17] Dong X, Liu O W, Howell A S, *et al.* An extracellular adhesion molecule complex patterns dendritic branching and morphogenesis. *Cell*, 2013, **155**(2): 296–307
- [18] Brenner J F, Dew B S, Horton J B, *et al.* An automated microscope for cytologic research. *J Histochem Cytochem*, 1971, **24**(1): 100–111
- [19] Russell M J, Douglas T S. Evaluation of autofocus algorithms for tuberculosis microscopy//29th International Conference of the IEEE EMBS, Engineering in Medicine and Biology Society, 2007: 3489–3492
- [20] Tenenbaum J M. Accommodation in Computer Vision, Ph.D. Thesis, (Stanford University), 1970
- [21] Krotkov E. Focusing. *Int J Comput Vision*, 1988, **1**(3): 223–237
- [22] Schlang J F, Sanderson A C, Neuman, *et al.* Implementation of automatic focusing algorithms for a computer vision system with camera control, Tech. Rep. CMU-RI-TR-83-14, Carnegie Mellon University, 1983

- [23] Jarvis R A. Focus optimization criteria for computer image processing. *Microscope*, 1976, **24**(2): 163-180
- [24] Geusebroek J, Frans C, Smeulders A W M, *et al.* Robust autofocusing in microscopy. *Cytometry*, 2000, **39**(1): 1-9
- [25] Subbarao M, Choi T, Nikzad A. Focusing techniques. *Opt Eng*, 1993, **32**(11): 2824-2836
- [26] Lee S Y, Kumar Y, Cho J M, *et al.* Enhanced autofocus algorithm using robust focus measure and fuzzy reasoning. *IEEE Trans Circ Syst Video Tech*, 2008, **18**(9): 1237-1246
- [27] Kautsky J, Flusser J, Zitovec B, *et al.* A new wavelet based measure of image focus. *Pattern Recogn Lett*, 2002, **23**: 1785-1794
- [28] Groen F, Young I T, Lighthart G. A comparison of different focus functions for use in autofocus algorithms. *Cytometry*, 1985, **6**(2): 81-91
- [29] Vollath D. Automatic focusing by correlative methods. *J Microsc*, 1987, **147**(3): 279-288
- [30] Vollath D. The influence of the scene parameters and of noise on the behaviour of automatic focusing algorithms. *J Microsc*, 1988, **151**(2): 133-146
- [31] Firestone L, Cook K, Culp K, *et al.* Comparison of autofocus methods for use in autofocus algorithms. *Cytometry*, 1991, **12**(3): 195-206
- [32] Zeder M, Perenthaler J. Multispot live-image autofocusing for high-throughput microscopy of fluorescently stained bacteria. *Cytometry*, 2009, **75A**(9): 781-788

自动对焦算法评估线虫脂滴图像的研究 *

张翔^{1, 2)}** 贾策²⁾ 谢康²⁾

¹⁾ 华中科技大学生命科学与技术学院, 武汉 430074; ²⁾ 中国科学院生物物理研究所, 北京 100101

摘要 自动对焦是实现线虫自动化筛选的一个重要步骤。在光学显微镜系统中, 通过采集同一个视野下不同焦面的图像, 再通过清晰度评价函数对这些图像进行运算, 得到的最大值被认为是最佳对焦位置。在本研究中, 对 16 种常用的自动对焦算法以及最近提出的一些算法进行了评估, 通过评估找出最适合线虫脂滴图像的自动对焦算法, 从而搭建一套线虫脂滴自动化筛选系统。同时就对焦精度、运算时间、抗噪声能力、对焦曲线等特征进行了分析评价, 结果表明, 大多数算法对线虫脂滴图像都有较好的表现, 特别是绝对 Tenengrad 算法在对焦精度上有最好的表现, 我们将优选该算法应用到线虫脂滴自动化筛选系统中。

关键词 线虫脂滴, 自动对焦算法, 自动化筛选

学科分类号 Q334, Q336

DOI: 10.16476/j.pibb.2015.0189

* 国家自然科学基金资助项目(31300701).

** 通讯联系人.

Tel: 010-64888522, E-mail: zhangxiang@moon.ibp.ac.cn

收稿日期: 2015-06-23, 接受日期: 2015-12-22